PAC Jeopardy Update to E12-13-008
Measuring Charged Pion Polarizability in the $\gamma\gamma \to \pi^+\pi^-$ Reaction

Spokespersons: I. Larin[1], D. Lawrence[2], R. Miskimen[1], and E.S. Smith[2]

and the Hall D GlueX Collaboration

[1] University of Massachusetts, Amherst MA 01003
[2] Thomas Jefferson National Accelerator Facility, Newport News VA 23606

June 22, 2020

Proposal Endorsed by the GlueX Collaboration

1 Overview of experimental goals and progress

Charged pion polarizability (CPP) is one of the important experimental tests of low-energy QCD [1]. The $O(p^4)$ prediction for the electric and magnetic polarizabilities is given by,

$$\alpha_\pi = -\beta_\pi = \frac{4\alpha}{m_\pi F_\pi^2}(L_9^r - L_{10}^r)$$

where the combination of low-energy constants $L_9^r - L_{10}^r$ is fixed by the ratio F_A/F_V in charged pion radiative decay, $\pi^+ \to e^+\nu\gamma$. The $O(p^6)$ corrections are predicted to be small.

While the prediction for CPP is very solid, there is considerable scatter among the experimental measurements, which typically suffer from low statistics and large systematic errors. Figure 1 shows a compilation of previous measurements of CPP. The $\gamma\gamma \to \pi^+\pi^-$ measurements were limited by sparse data, ≈ 200 data points for $W < 500$ MeV from Mark II [2], and the absence of an accurate theoretical model for $\gamma\gamma \to \pi\pi$.

The goal of the JLab experiment is to make a precision measurement of CPP by means of a high statistics study of the $\gamma\gamma \to \pi^+\pi^-$ reaction near 2π threshold. The two-photon cross section can be accessed in a tagged-photon measurement of $\gamma A \to \pi^+\pi^- A$ at very low momentum transfer through the Primakoff process

$$\frac{d^2\sigma}{d\Omega_{\pi\pi} dM_{\pi\pi}} = \frac{2\alpha Z^2}{\pi^2}\frac{E_\gamma^4\beta^2}{M_{\pi\pi}}\frac{sin^2\theta}{Q^4}|F(Q^2)|^2(1 + P_\gamma cos2\phi_{\pi\pi})\sigma(\gamma\gamma \to \pi\pi) \quad (1)$$

where $M_{\pi\pi}$ is the invariant mass of the 2π system, P_γ is the linear polarization of the incident beam, and $\phi_{\pi\pi}$ is the azimuthal angle of the $\pi\pi$ system. Figure 1 shows total cross sections from a subtracted dispersion theory calculation [3] for $\gamma\gamma \to \pi^+\pi^-$ for several values of $\alpha_\pi - \beta_\pi$. The sensitivity of the JLab experiment to $\alpha_\pi - \beta_\pi$ is of order $\pm 0.6 \times 10^{-4}\ efm^3$.

Since approval by PAC 40 the collaboration has been developing the detector and trigger upgrades needed for the experiment, as well as software tools for particle identification and

partial wave analysis. The engineering design for installation of the muon chambers and iron absorbers is also well underway. The report summarizes these efforts, as well as providing an update on recent measurements of CPP, and calculations for $\gamma\gamma \to \pi^+\pi^-$.

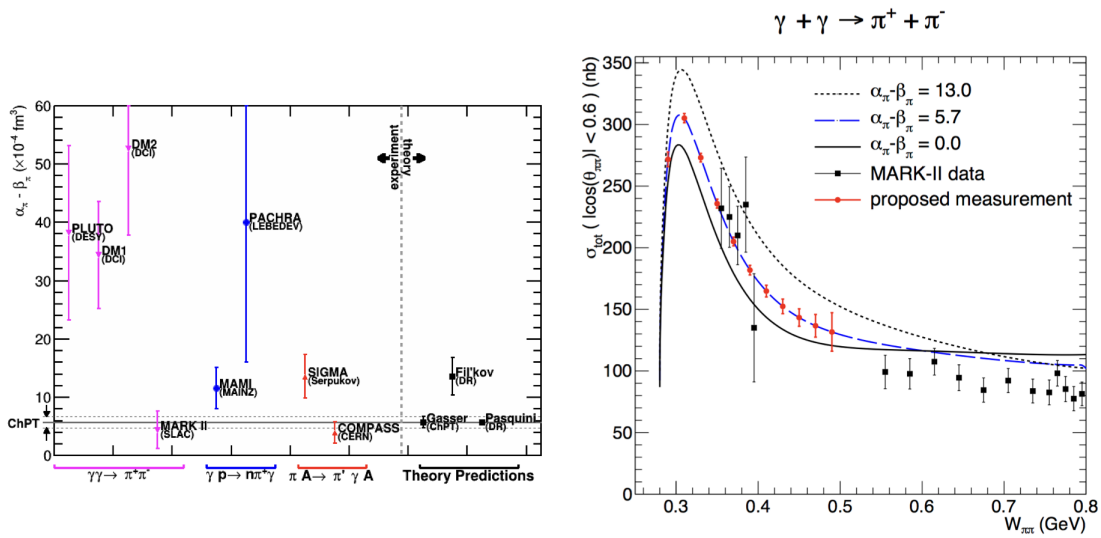

Figure 1: Left: measurements and calculations of the charged pion polarizability. Right: $\gamma\gamma \to \pi^+\pi^-$ cross sections.The solid, dashed and dotted curves are subtracted dispersion model calculations[3] with $\alpha_\pi - \beta_\pi$ equal to 0.0, 5.7 (ChPT), and 13.0, respectively. The black data points are from the Mark II [2], the red data points are projected data points from the JLab experiment.

2 Recent results for charged pion polarizability

The most recent measurements of CPP are radiative charged pion production at Mainz [4], and the COMPASS Primakoff experiment at CERN [5]. There has been much discussion of the "disagreement" of ChPT with Mainz, and the agreement with COMPASS, however both experiments agree with ChPT within two standard deviations. The COMPASS experiment measured Primakoff $\pi^- Ni \to \pi^-\gamma Ni$ production at $E_\pi = 60\ GeV$. The photon energy distribution dN_γ/dE_γ has sensitivity to α_π and β_π at the kinematic endpoint of the reaction, $E_\gamma \approx 60$ GeV, which is also a region where π^0 background is significant. The effect of nuclear coherent and incoherent reactions on the analysis, *i.e.* $\pi^- A \to \rho^- A \to \pi^-\gamma A$ and $\pi^- A \to \rho^- A \to \pi^-\pi^0 A$, is unexplored in the publication. The total absolute error

COMPASS obtained for $\alpha_\pi - \beta_\pi$ is $\pm 1.8 \times 10^{-4} e\ fm^3$. Given that the JLab and COMPASS experiments will have very different backgrounds and systematic errors, we conclude the two experiments are entirely complementary.

3 GEANT4 design studies for the muon detector

Design parameters of the muon chambers and absorbers were studied using a GEANT4-based simulation of different geometric configurations. A set of machine learning algorithms was used to determine the optimal μ/π separation for each geometrical configuration so they could be compared to one another. Figure 2 shows two such studies to optimize the size and shape of the deadened regions of the chambers and similarly for the beam hole size in the iron absorbers. This region will see the highest rates due to beam background, as well as signal events. Figure 3 shows a different simulation study which looks at the optimal μ/π separation for various numbers of absorbers and MWPCs. Each dot in each plot represents another geometry configuration (layer thicknesses and hole sizes). For each configuration an independent simulation was done and a TMVA model trained to optimize the separation for that configuration. The optimized design that fits behind FCAL and before the electronics racks is shown in Fig. 4. Not shown is a small "picture frame" lead shield in front of the lead absorber that can be adjusted in position so that the first aperture of the system is accurately centered on the beamline.

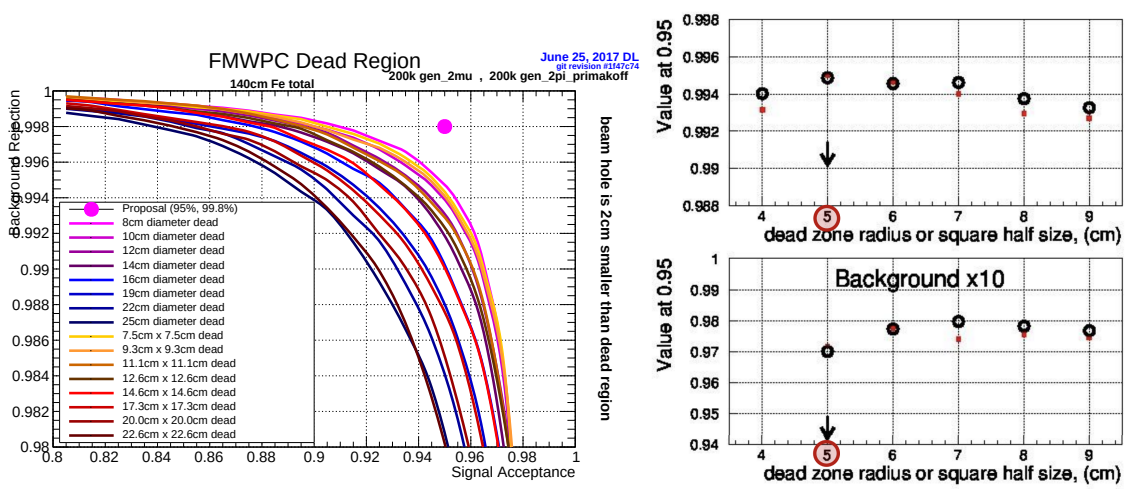

Figure 2: Left: Results of simulation study comparing dead regions of the muon chambers for both square and circular shapes of various sizes. Right: Simulation study optimizing the relative sizes of the dead region of the chambers and beam hole in the absorber. The red points are for square shapes and the black circles are for circular shapes. The bottom shows results if backgrounds are x10 greater than what s expected.

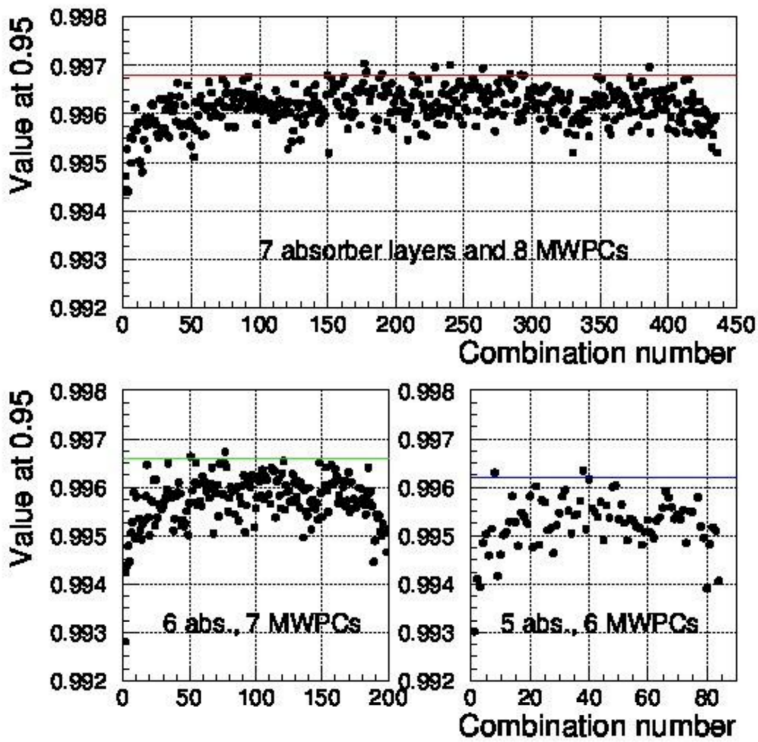

Figure 3: Result of a large simulation study comparing the μ/π separation (y-axis) for 95% signal acceptance for various geometric configurations. The x-axis is a number representing a particular configuration. The horizontal lines indicate the optimal separation geometry for the given number of absorbers and MWPCs.

4 Muon chamber construction and testing

Six muon chambers will be installed on the photon beamline, with the photon beam going through a deadened region in the center of the detectors. The detectors are shown in Figure 5. Relevant detector parameters are listed here: (1) wire geometry: $20\mu m$ sense wires alternating with $76\mu m$ field wires, 1 cm sense wire pitch, (2) chamber half-gap and active area: 1 cm, and 60×60 in^2, (3) central deadened region: 10×10 cm^2, (4) number of electronic channels: 144 , (5) biasing: sense wires at +1800 V, field wires and cathode planes @ ground, (6) operating gain: 10^5, (7) chamber gas: 90% Ar, 10% CO_2 by volume.

Seven of the eight muon chambers being built for the experiment have been completely strung. After wire stringing was completed we discovered that the 10 wires in the central deadened regions were noisy, producing a low voltage, $\sim$ 10 mV, discharge signal. Correcting the problem involves replacing the 10 central wires, a process that is well un-

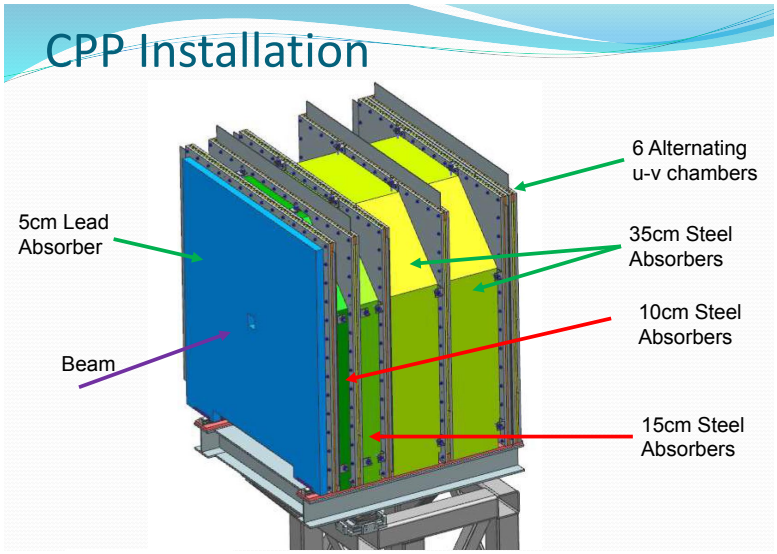

Figure 4: Layout of the MWPCs, lead and iron absorbers for the muon detector.

derway, 3 chambers have been rebuilt and have performed to our satisfaction. We expect the remaining 5 detectors will be ready by late summer or early fall 2020.

In early 2018 a full scale prototype chamber was installed on the Hall D beamline downstream of FCAL and the electronics racks. Data were taken during regular GlueX running using a trigger scintillator, and a $1/2 \times 12 \times 64$ in^3 iron absorber in front of the chamber for background studies. Figure 5 shows a photo of the detector installation. Despite large electromagnetic backgrounds, and the detector being essentially unshielded, the chamber operated reasonably well; scintillator triggers correlated with hits in the chamber, and the chamber didn't trip or draw large currents provided the photon beam tune was nominal. An oscillation was observed in the chamber electronics, not seen at UMass, and traced to a bad grounding connection between the aluminum cathode plates and the preamp electronics, since corrected.

5 Time-of-flight trigger for CPP

The trigger is organized the way it allows to select events with at least two charged particles reached the GlueX time-of-flight (TOF) system [6] consisting of two planes (vertically and horizontally oriented) of 46 scintillating paddles each. The paddles are combined in 16 groups per plane, each group has a signal if any of belonging paddles have a hit within 40 ns time window. The trigger condition is satisfied if at least two groups in both planes have a signal. This suits detecting requirements for charged pion or muon pairs perfectly. The optimal grouping pattern for the trigger efficiency and background rejection has been

Figure 5: Left: photograph of the eight muon chambers under construction at UMass. Right: prototype muon chamber installed at the end of the Hall D detector platform for beam tests

obtained from the simulations (fig. 6).

The main contribution to the expected trigger rate is coming from the electron-positron pair production in the target and downstream air. The rate value below 90 kHz is acceptable for the Hall-D DAQ system with livetime of 90% or more. The trigger rate test performed at December 2019 with the DIRC detector installed in front of the TOF showed low trigger rate ∼30 kHz that satisfies the requirements easily. To verify the results without the DIRC detector installed as it should be for the CPP experiment run we are planning to perform such a test during this summer run.

6 Muon chamber and absorber installation in Hall D

We are developing a solid CAD model of the structures that will be used to install and support the muon detector, which has an approximate weight of 20 tons. The plan is to install the muon detector downstream of the FCAL without unstacking the lead glass or removing the electronic racks. This is made possible by modifying the existing FCAL dark room by shortening it approximately 20" to allow sufficient room for the muon package to be inserted between the end of the modified dark room and the electronic racks. (The

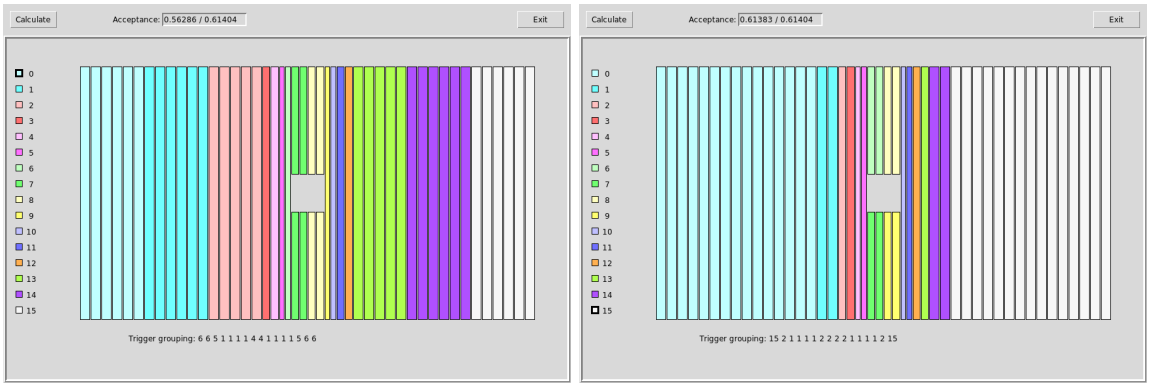

Figure 6: Two TOF paddles grouping schemes, each color represents different group. Left – original scheme, right – optimized with the acceptance

dark room is identified in red in Fig. 7 Left). This modification leaves a minimum of 20" of space to service FCAL PMTs. The weight of the muon detector is transferred by beams to Hilman rollers that move on plates on the floor of the hall (see Fig. 7 Right), allowing for the FCAL carriage to be moved for maintenance and installation/removal of the DIRC.

For installation each wire chamber will be attached and aligned to its respective iron plate on the floor of the hall. The chamber-plate assembly is then rigged onto rails that sit on the box support downstream of the dark room, and then pushed into position. The other chamber-plate assemblies are added sequentially.

7 Choice of nuclear target

When the CPP proposal was submitted the JLab PAC, the collaboration was considering the use of a medium weight nucleus as a target, for example an enriched isotope of Sn. Since then we've studied in detail how the choice of target can enhance the Primakoff signal relative to the $\gamma A \to \rho^0 A$ background, and the Primakoff signal relative to the nuclear coherent and incoherent backgrounds. From these studies we conclude ^{208}Pb is the optimal target for the CPP measurement. ^{208}Pb has closed proton and neutron shells, ground state $J^\pi = 0^+$, and a precisely measured charge density. The 5% radiation length enriched ^{208}Pb target used in the PrimEx-I experiment can be used for CPP.

8 Multivariate analysis for $e^\pm$, $\mu^\pm$ and $\pi^\pm$ identification

One of the primary backgrounds in CPP is Bethe-Heitler electrons. Studies of e/π separation were made using GlueX data with only two forward going tracks hitting the TOF. We used the ROOT TMVA package to train two neural nets: one for e-/π- classification,

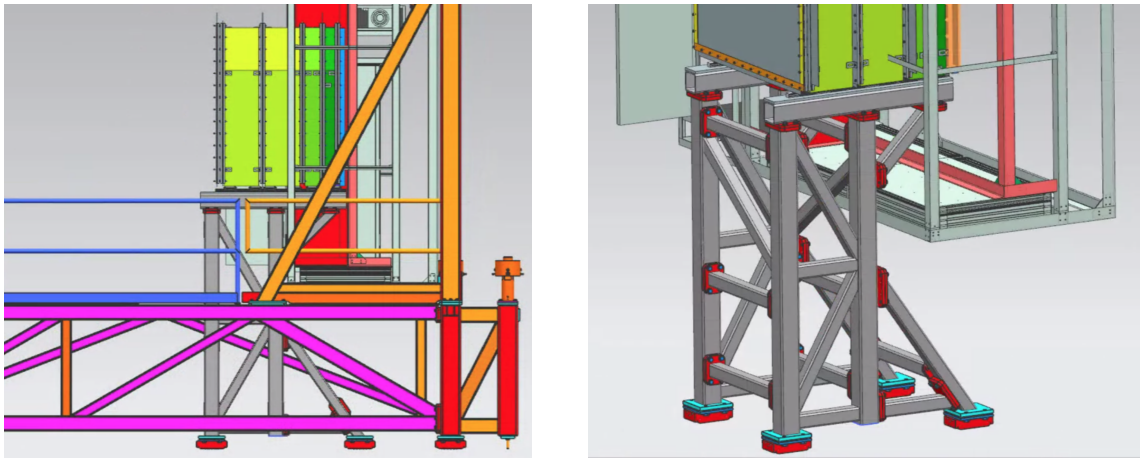

Figure 7: Schematic diagrams of CPP installation from the solid model. Left) The iron and muon chambers supported onto their position downstream of the FCAL. Right) Detail of the beams that are used to support the weight of the muon detector. Much of the existing structures and racks are removed for clarity.

and another for e+/π+. Each event has two neural net responses associated with it. Accepted events are those where *both* positive and negative tracks passed their individual neural net response cuts. For $e^{\pm}$ training we used Bethe-Heitler events from the Hall D hdgeant4 electron simulation, for $\pi^{\pm}$ training we used exclusive $p\pi^+\pi^-$ events at the ρ^0 peak from GlueX. The 4 training variables used are insensitive to differences between CPP kinematics and the training sample kinematics: (i) $E_{FCAL}/P_{kinematic-fit}$, (ii) FCAL DOCA (distance between the shower and track projection), (iii) FCAL E9/E25 shower ratio ("E9" and "E25" are the summed energies in a 3x3 and 5x5 array of PbG crystals centered on the shower), and (iv) the azimuthal angle of the track relative to the linear polarization direction. Figure 8 shows the input data before and after classification.

9 AmpTools for the analysis of CPP data

We have developed tools to extract the Primakoff signal using an amplitude analysis based on AmpTools.[1] As an illustration of this method, we have generated three sources of $\pi^+\pi^-$ pairs that are expected to dominate at threshold [7]: (i) the Primakoff signal (given by Eqn. 1), (ii) the $f_0(500)$ or σ meson, and (iii) the ρ-meson. The background amplitudes ($\mathcal{A}_\sigma$ and $\mathcal{A}_\rho$) are constructed as functions of the $\pi\pi$-mass, t, and the angular variables Φ, the production plane angle relative to photon polarization plane, and ϕ and θ, the emission

[1] AmpTools, https://github.com/mashephe/AmpTools/wiki.

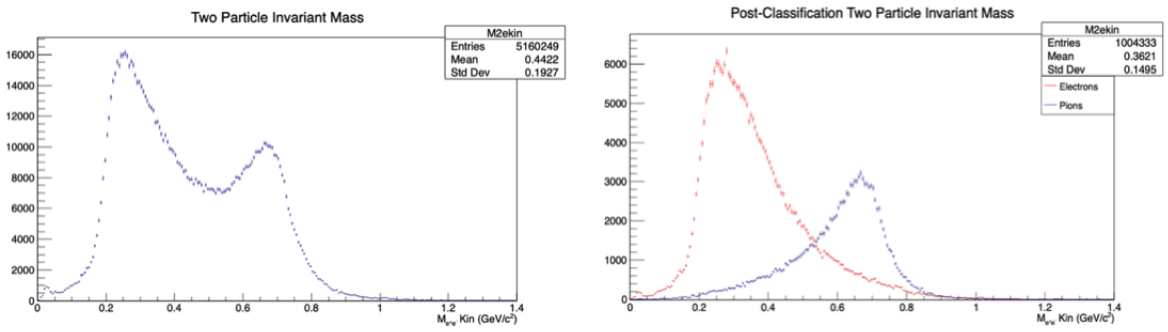

Figure 8: Left: input GlueX data containing both electrons and pions prior to classification. Right: the neural net applied to the input data twice, first selecting for pions (blue), then electrons (red).

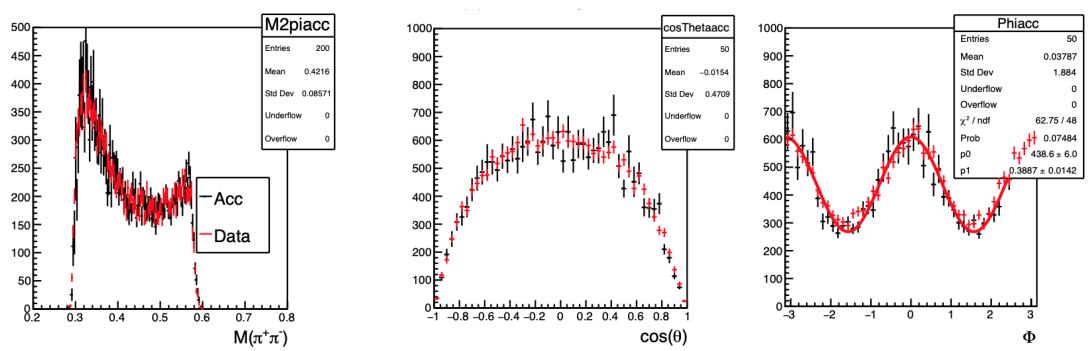

Figure 9: The Monte Carlo data sample is in red and the result of the amplitude fit is in black. Left) Events for $M_{\pi\pi} < 0.6$ GeV with the Primakoff signal peaking at threshold and the σ and ρ mesons contributing at higher mass. Center) The π^+ polar angle in the $\pi\pi$ rest frame, evidencing a P-wave and S-wave with poor acceptance at $\cos\theta = \pm 1$. Right) The signature $cos2\Phi$ distribution of the Primakoff signal.

angles in the $\pi\pi$ rest frame. The total intensity is then given by

$$\mathcal{I} \;=\; |a_P\mathcal{A}_P(m_{\pi\pi}, t, \Phi) + a_\sigma\mathcal{A}_\sigma(m_{\pi\pi}, t, \Phi) + a_\rho\mathcal{A}_\rho(m_{\pi\pi}, t, \Phi, \phi, \theta)|^2, \tag{2}$$

where a_i are fitted complex factors that represent the size of each contribution to the total intensity.

Signal and background amplitudes have different dependencies on the kinematic variables and the amplitude analysis performs an unbinned likelihood fit to determine the relative contributions of each amplitude to the data sample. We illustrate the procedure in Fig. 9 by displaying the distributions of some key variables of the Monte Carlo generated sample as well as the result of the fit. The fit is able to determine the relative contributions

of each source with good precision and there is good agreement between the "data" and the intensity calculated from the fitted amplitudes.

10 Theory update

Pasquini et al. [3] made the first state-of-the-art dispersion theory calculation for $\gamma\gamma \to \pi^+\pi^-$ and this calculation, shown in Figure 1 , was used in the preparation of the CPP proposal. Following approval of the CPP experiment by the JLab PAC, Dai and Pennington published a dispersion analysis for pion polarizabilies using their global analysis of $\gamma\gamma \to m^*m$ data [8]. Most recently, the the Mainz Prisma theory group established the calculation of vacuum polarization and hadronic light-by-light (HLbL) contributions to the muon $g-2$ magnetic moment as a high priority. Calculations of $\gamma^*\gamma^* \to \pi\pi$, with both incident photons virtual, are a key contribution to HLbL [9], [10],[11]. Given that $\gamma^*\gamma^* \to \pi\pi$ data are not available, measurements of $\gamma\gamma \to \pi\pi$ cross sections and polarizabilities from CPP and the proposed neutral pion polarizability experiment (NPP)[12] will provide a valuable constraint on the HLbL calculations.

References

[1] B. Holstein and S. Scherer. Hadron Polarizabilities. *arXiv:1401.0140v1 [hep-ph]*, 2014.

[2] J. Boyer et al. *Phys. Rev. D*, 42:1350, 1990.

[3] D. Drechsel B. Paquini and S. Scherer. *Phys. Rev. C*, 77:06521, 2008.

[4] J. Ahrens et al. *Eur. Phys. J A*, 23:113, 2005.

[5] C. Adolph et al. *Phys. Rev. Lett.*, 114:062002, 2015.

[6] P.M. Eugenio. TOF upgrade. Technical Report GlueX-doc-**4023**, Jefferson Lab, May 2019.

[7] E.S. Smith. CPP Update: Coherent hadronic S-wave production. Technical Report GlueX-doc-**3803**, Jefferson Lab, October 2018.

[8] L.Y. Dai and M.R. Pennington. *Phys. Rev. D*, 94:116021, 2016.

[9] M. Vanderhaeghen I. Danilkin. *Phys. Lett. B*, 789:366, 2019.

[10] M. Vanderhaeghen I. Danilkin, C. Redmer. *Prog. Part. Nucl. Phys.*, 107:20, 2019.

[11] M. Vanderhaeghen I. Danilkin, O. Deineka. *Phys. Rev. D*, 101:054008, 2020.

[12] M. Ito et al. Proposal to JLab PAC 48: Measuring the Neutral Pion Polarizability, 2020.